

# Focused Limited-Diffraction Beams for Ultrasound Therapy Applications

Jian-yu Lu

Ultrasound Lab, Department of Bioengineering, The University of Toledo  
Toledo, OH 43606, USA  
Email: [jian-yu.lu@ieee.org](mailto:jian-yu.lu@ieee.org)

**Abstract** – Limited-diffraction beams (LDBs) such as Bessel beams and X waves have been studied since late 1980s and early 1990s respectively. These beams have a large depth of field and were applied mainly for medical imaging. (For example, LDBs can maintain a narrow -6-dB beam width of about 2.54 mm in water from the surface of the transducer to more than 200 mm depth at a frequency of 2.5 MHz.) In these applications, LDBs were not focused in order to have a large depth of field.

In this paper, both focused zeroth-order and higher-order LDBs were studied for ultrasound therapy applications. The advantage of using focused LDBs is that their focal areas and shapes can be systematically controlled to treat tumors of various sizes.

In the study, Bessel beams of 2.5 MHz were produced with a 50 mm diameter transducer. The Bessel beams were focused at 50 mm depth and the sizes and shapes of the focal areas were controlled by the scaling parameter and the order of the Bessel beams. To increase the total transmitting power and reduce the number of elements of the transducer needed to produce the Bessel beams, the amplitudes of the lobes of the Bessel beams can be quantized at the surface of the transducer.

Results show that with the focused Bessel beams, the sizes of the focal areas increase with the increase of the Bessel scaling parameter, and higher-order Bessel beams produce a perforated focus area.

**Keywords** – *Focused Limited-Diffraction Beams, Limited-Diffraction Beams, Bessel Beams, High-order Bessel Beams, Ultrasound Therapy, Focused Ultrasound*

## I. INTRODUCTION

Traditionally, focused plane-wave transducers are used in ultrasound therapy [1]. The focal spot of such transducers is very small. However, in some therapy applications, there is a need to increase the focal area or change its shape. For example, if the size of a tumor is larger than the small focal spot of a focused plane wave, it is advantageous to use a larger focus to cover the entire area of the tumor for treatment. To increase the size of the focal area at a given focal depth, the size of the focused plane-wave transducer must be reduced, which reduces the total power and is undesirable [2].

Unfocused limited-diffraction beams (LDBs) such as Bessel beams [3-5] and X waves [6-7] have been studied extensively for medical imaging due to their large depth of

field [8-9]. For example, a Bessel beam produced by a 50 mm diameter transducer can maintain a narrow -6-dB beam width of about 2.54 mm in water from the surface of the transducer to a depth of more than 200 mm at a frequency of 2.5 MHz [5]. However, focused LDBs have not been studied because they will reduce the depth of field. In this paper, LDBs were focused to control the sizes and shapes of the focal areas for ultrasound therapy applications.

## II. METHOD

2.5-MHz (about 0.6-mm wavelength in water) zeroth-, first-, and third-order Bessel beams [6] were produced with a 50-mm diameter transducer and were focused at 50 mm depth (using a lens) by weighting the transducer surface with Bessel functions  $J_0(\alpha r)$ ,  $J_1(\alpha r)\cos(\varphi)$ , and  $J_3(\alpha r)\cos(3\varphi)$  respectively, where  $\alpha$  is the scaling parameter that determines the size of the focal area of the beams,  $r$  is the radial distance from the center of the transducer,  $0 \leq \varphi \leq 2\pi$  is the angle around the axis of the beam, and  $J_0()$ ,  $J_1()$ , and  $J_3()$  are the zeroth-, first-, and third-order Bessel functions of the first kind. Two values of the scaling parameter of the Bessel beams were used:  $\alpha = 0.125b$  and  $\alpha = 0.25b$ , where  $b = 1202.45 \text{ m}^{-1}$  is a constant used in [5]. To increase the transmission power, the amplitudes of the lobes of the Bessel functions were modified at the surface of the transducer. One modification was for the zeroth-order Bessel beam with  $\alpha = 0.125b$ , where  $J_0(\alpha r)$  function was set to 0.4 when  $J_0(\alpha r) \geq 0.4$  and  $J_0(\alpha r)$  was set to -0.4 when  $J_0(\alpha r) \leq -0.4$ . For the zeroth-order Bessel beam with  $\alpha = 0.25b$ , the limit values  $\pm 0.4$  were changed to  $\pm 0.3$ . The amplitudes of the modified Bessel functions at the transducer surface were then normalized  $\pm 1.0$ . I.e., after normalization,  $\pm 0.4$  and  $\pm 0.3$  values all become  $\pm 1.0$ .

To further increase the transmitting power and reduce the number of transducer elements, binary modifications to the Bessel functions were made on the transducer surface to produce modified Bessel beams. I.e.,  $J_0(\alpha r)$ ,  $J_1(\alpha r)\cos(\varphi)$ , and  $J_3(\alpha r)\cos(3\varphi)$  were set to 1.0 if they were zero or positive and were set to -1.0 if they were negative.

## III. RESULTS

The simulation results using the parameters above are given in the figures below. In the simulation, the 50-mm diameter transducer was divided into 512x512 rectangular squares. The

ultrasound beams were simulated efficiently using the method given in [10], which can be used to produce any three-dimensional (3D) wave fields of a 2D array transducer.

Figs. 1(a) and (d) show the normalized magnitudes of the transverse profiles of the ultrasound pressure at the axial distance of 0 mm (at the surface of the transducer) and 50 mm (the focal distance) for the plane wave focused with a lens. Notice that in ultrasound therapy applications, the intensity of the beams is of interest (the intensity is the square of the pressure and thus has a lower sidelobe than what is displayed). Figs. 1(b) and (e) are the same as those of Figs. 1(a) and (d) respectively except that the beams were produced with modified (+/-0.4 modifications) focused  $J_0(ar)$  Bessel beams with  $\alpha = 0.125b$ . Figs. 1(c) and (f) are the same as those of Figs. 1(b) and (e) respectively except that  $\alpha = 0.25b$  and the modification values are +/-0.3.

The plots of the normalized magnitudes of the transverse beam profiles through the center of the beams at depths of 0 mm and 50 mm are shown in Fig. 2(a) and 2(b) respectively. The solid lines, dashed lines, and dotted lines are for focused plane wave (Figs. 1(a) and (d)), modified focused  $J_0(ar)$  Bessel beam with  $\alpha = 0.125b$  (Figs. 1(b) and (e)), and modified focused  $J_0(ar)$  Bessel beam with  $\alpha = 0.25b$  (Figs. 1(c) and (f)), respectively.

The normalized magnitudes of the axial beam profiles along the axis of the transducer from depths of 0 mm to 120 mm for the focused plane wave (Figs. 1(a) and (d)), modified focused  $J_0(ar)$  Bessel beam with  $\alpha = 0.125b$  (Figs. 1(b) and (e)), and modified focused  $J_0(ar)$  Bessel beam with  $\alpha = 0.25b$  (Figs. 1(c) and (f)) are shown in Fig. 3(a), 3(b), and 3(c), respectively.

To further increase the transmission power and reduce the number of transducer elements, binary modifications to the focused Bessel beams were produced.

Figs. 4(a) and (b) show the normalized magnitudes of transverse beam profiles of the 2.5-MHz, binary-modified, and focused zeroth-order Bessel beams  $J_0(ar)$  measured at 50 mm (focal distance) with  $\alpha = 0.125b$  and  $0.25b$  respectively. Figs. 4(c) and (d) are the same as Figs. 4(a) and (b) respectively except that the Bessel beams were not modified. Figs. 5(a), (b), (c), and (d) are the normalized magnitudes of the axial beam profiles of the beams from 0 mm to 120 mm along the center of

the transducer (the transducer was at the left end of the beam profiles) corresponding to Figs. 4(a), (b), (c), and (d) respectively.

Figs. 6(a), (b), (c), and (d) are the same as Figs. 4(a), (b), (c), and (d) respectively except that the first-order Bessel beams  $J_1(ar)\cos(\varphi)$  were produced [6]. Figs. 7(a), (b), (c), and (d) are the same as Figs. 5(a), (b), (c), and (d) respectively except that they are the results of the first-order Bessel beams.

Figs. 8(a), (b), (c), and (d) are the same as Figs. 6(a), (b), (c), and (d) respectively except that the third-order Bessel beams  $J_3(ar)\cos(3\varphi)$  were produced [6]. Figs. 9(a), (b), (c), and (d) are the same as Figs. 7(a), (b), (c), and (d) respectively except that they are the results of the third-order Bessel beams.

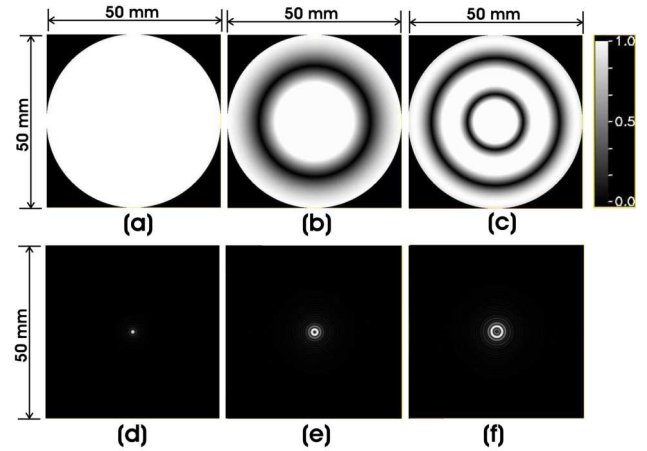


**Figure 1.** Modified 2.5-MHz focused zeroth-order Bessel beams  $J_0$  in comparison with a focused plane wave. (a) and (d) are normalized magnitudes of transverse beam profiles of a focused plane wave at distance 0 mm and 50 mm (focal distance) away from the surface of the transducer respectively. (b) and (e) are the same as (a) and (d) respectively except that they were produced with a modified (setting  $J_0(ar)$  to 0.4 if  $J_0(ar) \geq 0.4$  and setting  $J_0(ar)$  to -0.4 if  $J_0(ar) \leq -0.4$  to increase the transmitting power) focused Bessel beam with  $\alpha = 0.125b$ , where  $b = 1202.45 \text{ m}^{-1}$ . (c) and (f) are the same as (b) and (d) respectively except that  $\alpha = 0.25b$  (modified by setting  $J_0(ar)$  to 0.3 if  $J_0(ar) \geq 0.3$  and setting  $J_0(ar)$  to -0.3 if  $J_0(ar) \leq -0.3$  to increase the transmitting power). The diameter (50 mm) of the transducer is shown in the figure.

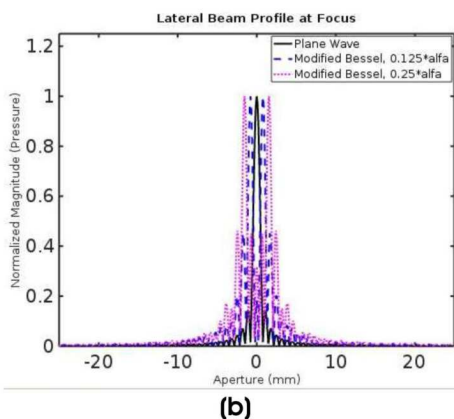
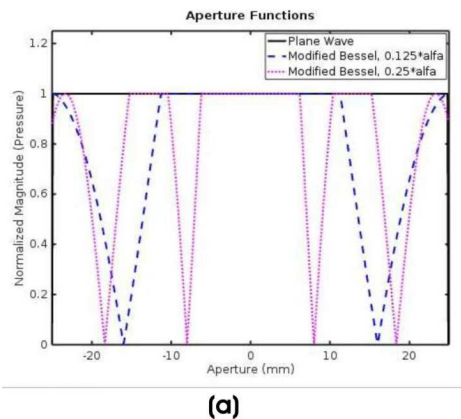


**Figure 2.** Normalized magnitudes of the transverse beam plots corresponding to the beams in Fig. 1 through the center of the transducer at depth of (a) 0 mm (surface of the transducer) and (b) 50 mm (the focal distance). The solid lines, dashed lines, and dotted lines represent the beam plots of the focused plane wave, modified focused  $J_0(ar)$  Bessel beam with  $\alpha = 0.125b$ , and modified focused  $J_0(ar)$  Bessel beam with  $\alpha = 0.25b$ , respectively.

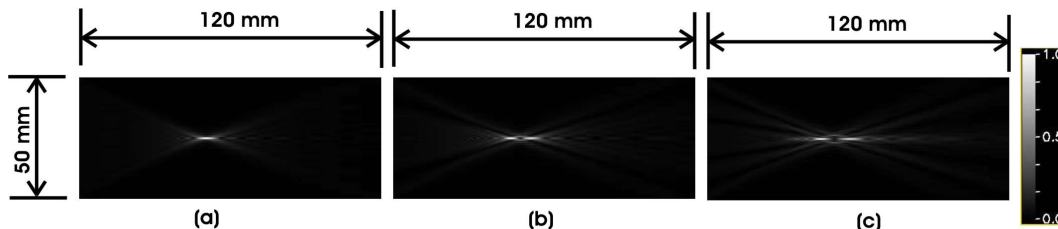


**Figure 3.** Axial beam profiles of the normalized magnitude of the beams corresponding to those in Fig. 1 along the axis of the transducer of the focused plane wave (a), modified focused  $J_0(ar)$  Bessel beam with  $\alpha = 0.125b$  (b), and modified focused  $J_0(ar)$  Bessel beam with  $\alpha = 0.25b$  (c).

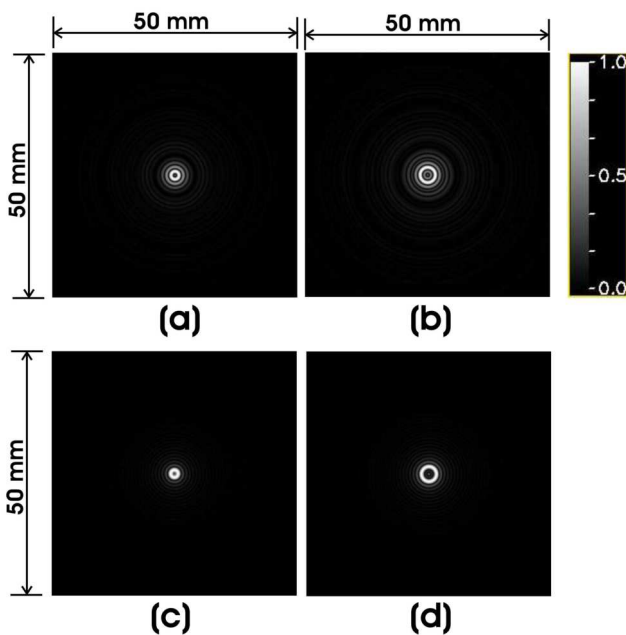


**Figure 4.** (a) and (b) are normalized magnitudes of transverse beam profiles of 2.5-MHz focused zeroth-order Bessel beams  $J_0(ar)$  measured at 50 mm (focal distance) with  $\alpha = 0.125b$  and  $0.25b$  respectively, where  $b = 1202.45 \text{ m}^{-1}$ . The Bessel beams were modified at the surface of the transducer by setting  $J_0(ar)$  to 1.0 if  $J_0(ar) \geq 0$  and setting  $J_0(ar)$  to -1.0 if  $J_0(ar) < 0$  to maximize the transmitting power and reduce the number of transducer elements. (c) and (d) are the same as (a) and (b) respectively except that the Bessel beams were not modified. The dimensions of the images are shown in the figure.

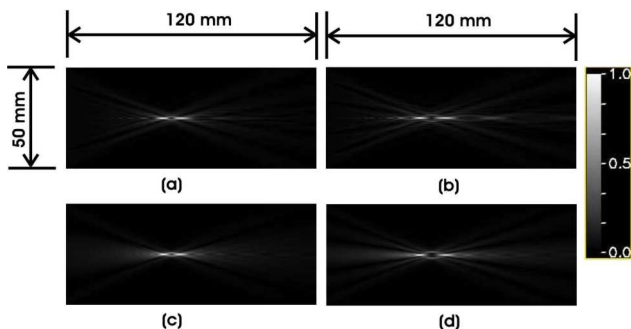


**Figure 5.** (a), (b), (c), and (b) are the axial beam profiles of the normalized magnitudes of the beams in Fig. 4 along the center of the transducer (the transducer was at the left end of the beam profiles). The dimensions of the images are shown in the figure.

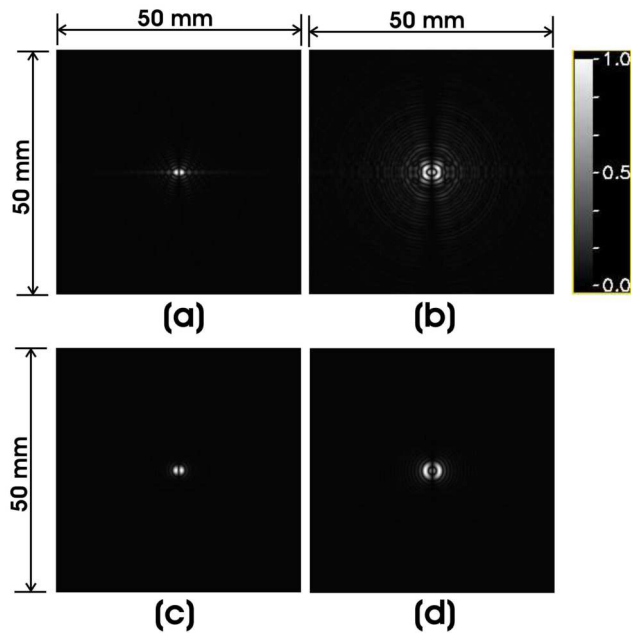


**Figure 6.** (a) and (b) are normalized magnitudes of transverse beam profiles of 2.5-MHz focused 1st-order Bessel beams  $J_1(ar)\cos(\varphi)$  measured at 50 mm (focal distance) with  $\alpha = 0.125b$  and  $0.25b$  respectively, where  $b = 1202.45 \text{ m}^{-1}$  and  $-\pi \leq \varphi \leq \pi$  is an angle around the beam axis. The Bessel beams were modified at the surface of the transducer by setting  $J_1(ar)\cos(\varphi)$  to 1.0 if  $J_1(ar)\cos(\varphi) \geq 0$  and setting  $J_1(ar)\cos(\varphi)$  to -1.0 if  $J_1(ar)\cos(\varphi) < 0$  to maximize the transmitting power and reduce the number of transducer elements. (c) and (d) are the same as (a) and (b) respectively except that the Bessel beams were not modified. The dimensions of the images are shown in the figure.

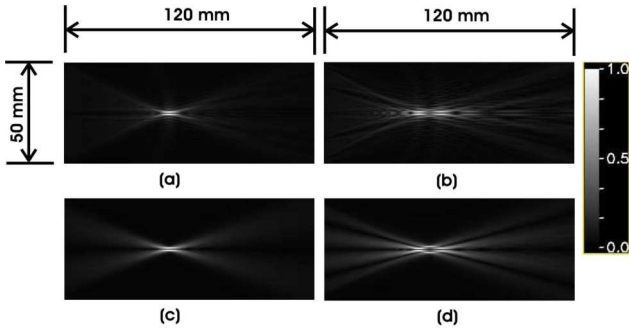


**Figure 7.** (a), (b), (c), and (d) are the axial beam profiles of the normalized magnitudes of the beams in Fig. 6 along the center of the transducer at  $\varphi = 0$  (the transducer was at the left end of the beam profiles). The dimensions of the images are shown in the figure.

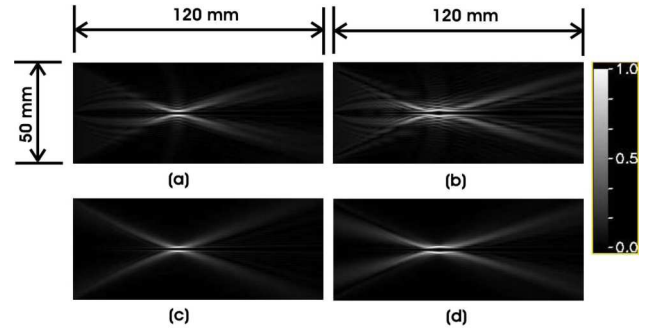


**Figure 9.** (a), (b), (c), and (d) are the axial beam profiles of the normalized magnitudes of the beams in Fig. 8 along the center of the transducer at  $\varphi = 0$  (the transducer was at the left end of the beam profiles). The dimensions of the images are shown in the figure.

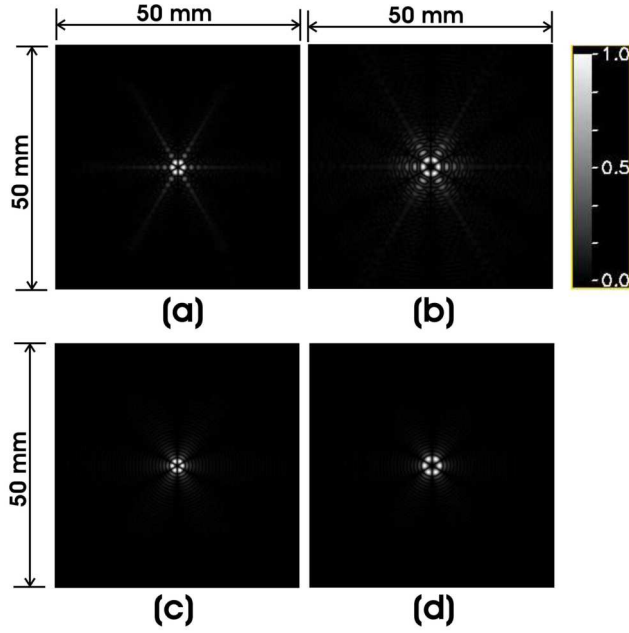


**Figure 8.** (a) and (b) are normalized magnitudes of transverse beam profiles of 2.5-MHz focused 3rd-order Bessel beams  $J_3(ar)\cos(3\varphi)$  measured at 50 mm (focal distance) with  $a = 0.125b$  and  $0.25b$  respectively, where  $b = 1202.45 \text{ m}^{-1}$  and  $-\pi \leq \varphi \leq \pi$  is an angle around the beam axis. The Bessel beams were modified at the surface of the transducer by setting  $J_3(ar)\cos(3\varphi)$  to 1.0 if  $J_3(ar)\cos(3\varphi) \geq 0$  and setting  $J_3(ar)\cos(3\varphi)$  to -1.0 if  $J_3(ar)\cos(3\varphi) < 0$  to maximize the transmitting power and reduce the number of transducer elements. (c) and (d) are the same as (a) and (b) respectively except that the Bessel beams were not modified. The dimensions of the images are shown in the figure.

#### IV. CONCLUSION

It is clear from the results that the size of the focal area can be controlled in both transverse and axial directions with the focused Bessel beams by changing its scaling parameters and/or orders. When the Bessel functions are quantized at the transducer surface, the transmission power is increased and the number of transducer elements can be reduced without significantly changing the beam profiles.

#### REFERENCES

- [1] Zahra Izadifar, Zohreh Izadifar, Dean Chapman, and Paul Babyn, "An Introduction to High Intensity Focused Ultrasound: Systematic Review on Principles, Devices, and Clinical Applications," *Journal of Clinical Medicine*, vol. 9, no. 2, pp. 460, February 2020.
- [2] Libertario Demi, "Practical Guide to Ultrasound Beam Forming: Beam Pattern and Image Reconstruction Analysis," *Applied Sciences*, vol. 8, no. 1544, pp. 1-15, September 3, 2018.
- [3] J. Durnin. "Exact solutions for nondiffracting-beams. I. The scalar theory." *Journal of Optical Society of America*, vol. 4, no. 4, pp. 651-654, 1989.
- [4] D. K. Hsu, F. I. Marccclan, and D. O. Thompson. "Bessel beam ultrasonic transducer: Fabrication method and experiment results" *Applied Physics Letter*, vol. 55, no. 2066, November, 1989.
- [5] Jian-yu Lu and J. F. Greenleaf, "Ultrasonic nondiffracting transducer for medical imaging," *IEEE Transactions on Ultrasonics, Ferroelectrics, and Frequency Control*, vol. 37, no. 5, pp. 438-447, September 1990.
- [6] Jian-yu Lu and J. F. Greenleaf, "Nondiffracting X waves --- exact solutions to free-space scalar wave equation and their finite aperture realizations," *IEEE Transactions on Ultrasonics, Ferroelectrics, and Frequency Control*, vol. 39, no. 1, pp. 19-31, January 1992.
- [7] Jian-yu Lu and J. F. Greenleaf, "Experimental verification of nondiffracting X waves," *IEEE Transactions on Ultrasonics, Ferroelectrics, and Frequency Control*, vol. 39, no. 3, pp. 441-446, May 1992.
- [8] Jian-yu Lu, Hehong Zou, and J. F. Greenleaf, "Biomedical ultrasound beam forming," *Ultrasound in Medicine and Biology*, vol. 20, no. 5, pp. 403-428, July 1994.
- [9] Jian-yu Lu, Hehong Zou, and J. F. Greenleaf, "Biomedical ultrasound beam forming," *Ultrasound in Medicine and Biology*, vol. 20, no. 5, pp. 403-428, July 1994.
- [10] Jian-yu Lu and Jiqi Cheng, "Field computation for two-dimensional array transducers with limited diffraction array beams," *Ultrasonic Imaging*, vol. 27, no. 4, pp. 237-255, October 2005.